Cosmic dawn:
Objects in the era of re-ionization

review and future perspective

Masayuki Akiyama

(Astronomical Institute, Tohoku Univ.)

Re-ionization of the Universe

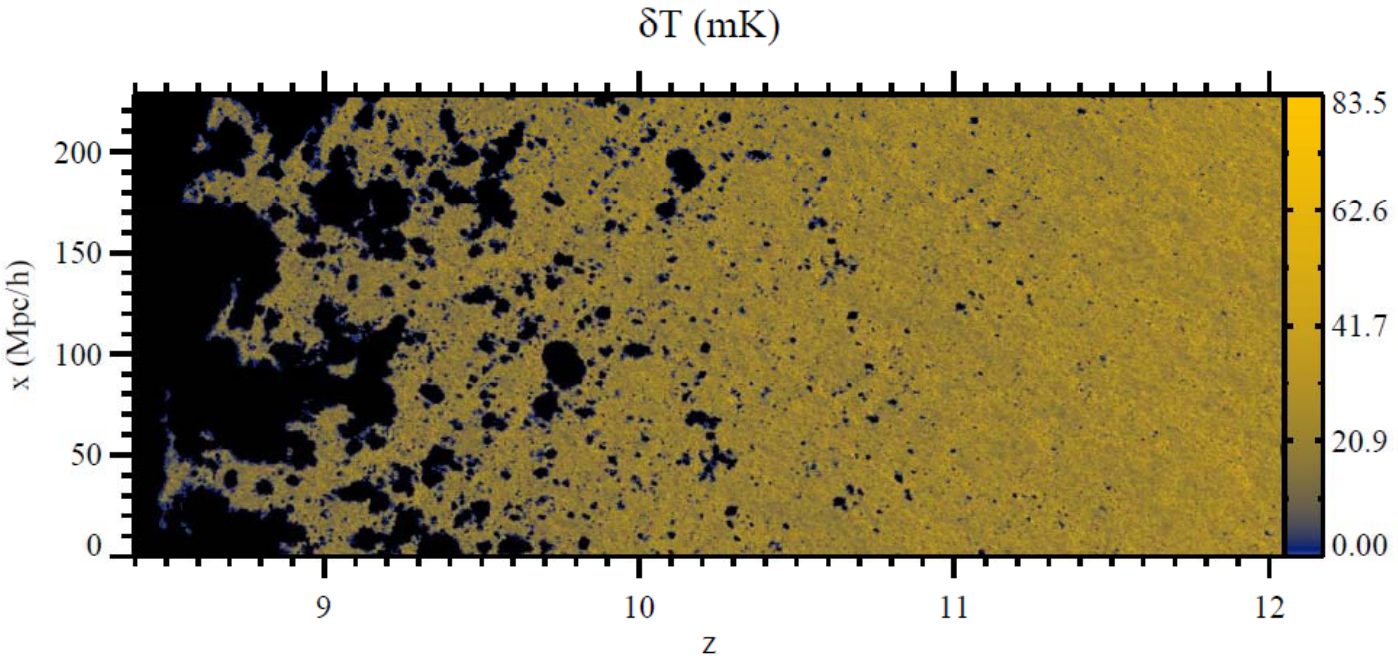

N-body + radiative transfer simulation of HI 21cm line brightness temperature fractuation by Iliev et al. 2012

Current observational challenges are to reveal…

- When ?
- What ?
  - Galaxies or AGNs ? = stars or black holes ?
  - Massive galaxies or less-massive galaxies ?
- How ?
  - Escape fraction of ionizing photons from galaxies
  - Clumping factor of IGM

When ?

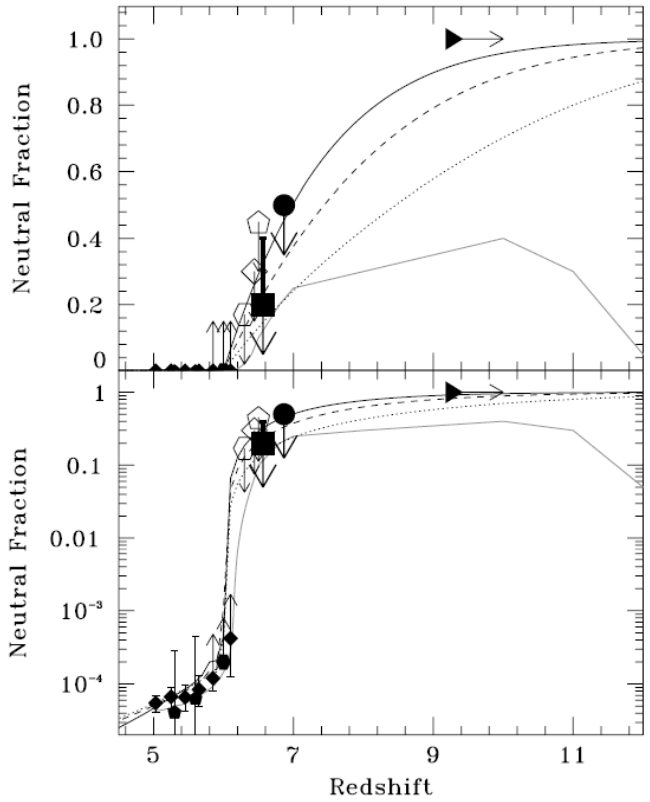

Figure 23. Neutral-hydrogen fraction, $x_{\rm H\,I}$, of IGM as a function of redshift. Top and bottom panels are the same, but with a vertical axis of linear and log scales, respectively. The filled square and circle are the upper limits of $x_{\rm H\,I}$ that we obtain from the evolution of Lyα LF and clustering, respectively. The open diamond and pentagon denote the upper limits from Lyα LF at $z = 6.5$ given by Malhotra & Rhoads (2004) and Kashikawa et al. (2006). The open hexagon is the upper limit estimated from the constraints of Lyα damping wing of GRB at $z = 6.3$ (Totani et al. 2006), respectively. The filled hexagon and pentagons indicate constraints given by GRB spectra (Gallerani et al. 2008b) and QSO dark gap statistics (Gallerani et al. 2008a), respectively. The filled diamonds represent the measurements from GP optical depth of SDSS QSOs (Fan et al. 2006). The triangle plots the 1σ lower limit of redshift of a neutral universe given by WMAP7 (Larson et al. 2010) in the case of instantaneous reionization. Avoiding overlapping symbols, we give a small offset along redshift to the positions of the filled circle and the open diamond. Dotted, dashed, and solid lines show the evolution of $x_{\rm H\,I}$ for minihalo, small, and large halo cases, respectively, predicted by Choudhury et al. (2008). Gray solid line presents the prediction in the double reionization scenario suggested by Cen (2003).

Observational constraints on the neutral fraction as a function of redshift.

Ouchi et al. 2010

When ?

Constraint on the neutral hydrogen fraction from the spectrum of z=6.3 GRB (this case the cutoff is likely dominated by damped Ly-alpha absorption by its host galaxy and upper limit on the neutral fraction).

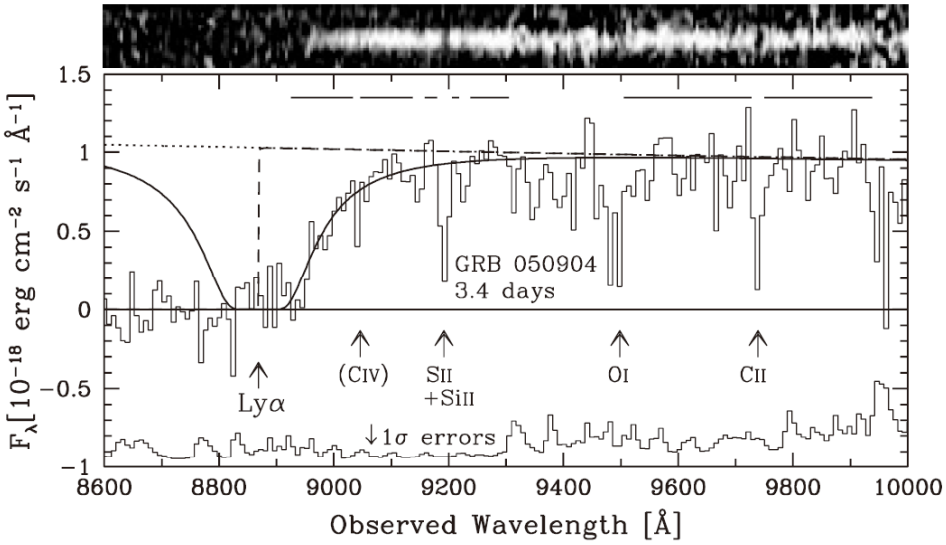

Fig. 1. Afterglow spectrum of GRB 050904 taken 3.4 days after the burst. The spectrum is binned by 3 pixels, and 1σ errors are also shown with an offset of -1.0. The CCD image of the spectrum in the corresponding wavelength range is shown at the top of the figure. The Lyα resonance and identified absorption lines are indicated with the redshift $z_{\rm metal} = 6.295$, except for the intervening C IV system at $z = 4.840$. The thick horizontal lines in the upper right region show the wavelength ranges used in the spectral fitting, where identified absorption features are removed. The solid curve shows the model absorption by a DLA with $\log N_{\rm H\,I} = 21.62$ and $z_{\rm DLA} = 6.295$ (the DLA-dominated model). The dotted curve shows the original unabsorbed spectrum of the afterglow, with the spectral index of $\beta_0 = -1.25$. The dashed curve shows the model absorption by an IGM with $z_{\rm IGM,u} = 6.295$ and $x_{\rm H\,I} = 10^{-3}$, which is almost a vertical line at the Lyα resonance. The Galactic extinction of $E(B-V) = 0.060$ mag is taken into account in all the model curves.

Totani et al. 2006

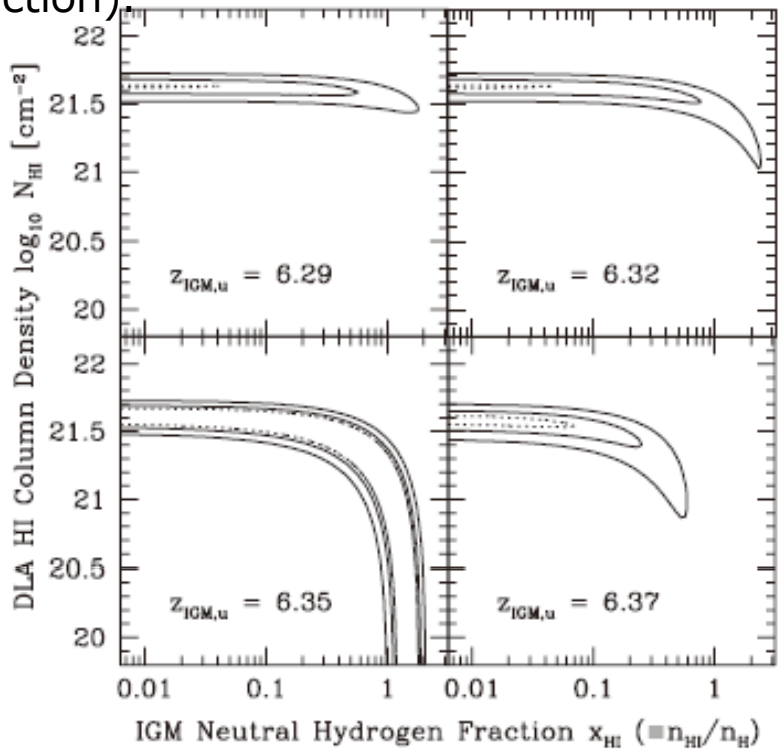

Fig. 5. Allowed regions are for a joint fit of the DLA and IGM absorption models. The four panels are for different values of $z_{\rm IGM,u}$ as indicated in the panels. The DLA redshift is fixed to $z_{\rm DLA} = z_{\rm metal} = 6.295$. The contours show the levels of $\Delta\chi^2 = 3.53$, 11.3, and 21.1 from the minimum χ^2, corresponding to 95 (dotted), 99 (thick solid), and 99.99% (thin solid) confidence levels for three degrees of freedom. See text (section 3) for the reason why the apparently unphysical region of $x_{\rm H\,I} > 1$ is shown.

When ?

Sight lines to even higher redshifts available with GRBs.

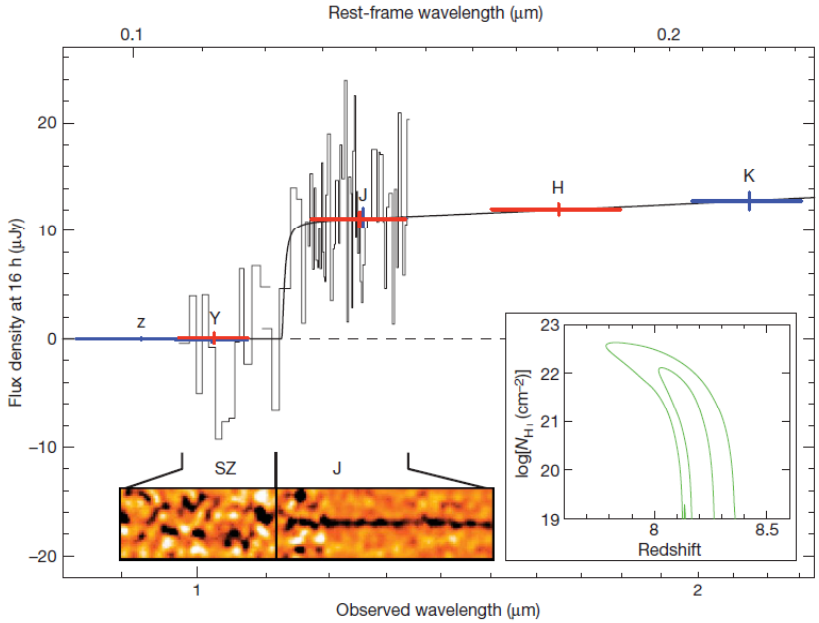

Figure 2 | The composite infrared spectrum of the GRB 090423 afterglow. SZ-band (0.98–1.1 μm) and J-band (1.1–1.4 μm) one- and two-dimensional spectra obtained with the VLT using the Infrared Spectrometer And Array Camera (ISAAC). Also plotted are the sky-subtracted photometric data points obtained using Gemini North's NIRI (red) and the VLT's High Acuity Wide field K-band Imager and Gemini South's Gemini Multi-Object Spectrograph (blue) (scaled to 16 h after the burst and expressed in microjanskys; 1 Jy = 10^{-26} W m^{-2} Hz^{-1}). The vertical error bars show the 2σ (95%) confidence level, and the horizontal lines indicate the widths of the filters. The shorter-wavelength measurements are non-detections, and emphasize the tight constraints on any transmitted flux below the break. The break itself, at an observed wavelength of about 1.13 μm, is seen to occur close to the short-wavelength limit of the J-band spectrum, below which, although noisy, the spectrum shows no evidence of any detected continuum. Details of the data-reduction steps and adaptive binning used to construct these spectra are given in Supplementary Information. A model spectrum showing the H I damping wing for a host galaxy with a hydrogen column density of $N_{H\,I} = 10^{21}$ cm^{-2} at a redshift of $z = 8.23$ is also plotted (solid black line), and provides a good fit to the data. Inset, allowing for a wider range in possible host $N_{H\,I}$ values gives the 1σ (68%) and 2σ confidence contours shown. The fact that no deviation is seen from a power-law spectrum at wavelengths greater than 1.2 μm, together with its shallow spectral slope, suggests that there is little or no dust along the line of sight through the GRB host galaxy (unless it is 'grey'), consistent with the galaxy being relatively unevolved, and having a low abundance of metals.

GRB at z~8.2
Tanvir et al. 2009

When ?

The size of the ionized region around z~7 QSOs can also constrain IGM neutral fraction (this case again can be explained with damped Ly-alpha system with 4x10^20cm2 in the line of sight).

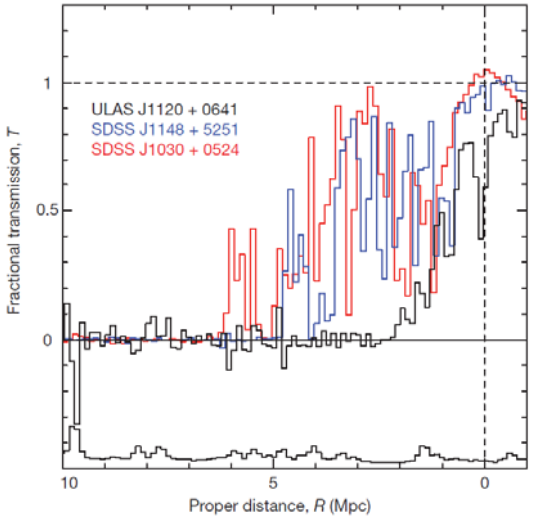

Figure 3 | The inferred Lyα near-zone transmission profile of ULAS J1120+0641 compared to those of two lower-redshift quasars. The near-zone transmission profile of ULAS J1120+0641 was estimated by dividing the observed spectrum by the composite spectrum shown in Fig. 1 and the conversion from wavelength to proper distance was calculated for a fiducial flat cosmological model[9]. The transmission profiles towards the two SDSS quasars were estimated by dividing their measured[29] spectra by parameterized fits based on the unabsorbed spectra of lower-redshift quasars. The transmission profile of ULAS J1120+0641 is strikingly different from those of the two SDSS quasars, with a much smaller observed near-zone radius R_{NZ}, as well as a distinct shape: whereas the profiles of SDSS J1148+5251 and SDSS J1030+0524 have approximately Gaussian envelopes out to a sharp cut-off, the profile of ULAS J1120+0641 is much smoother and also shows absorption redward of Lyα. The 1σ error spectrum for ULAS J1120+0641 is shown below the data.

Mortlock et al. 2011

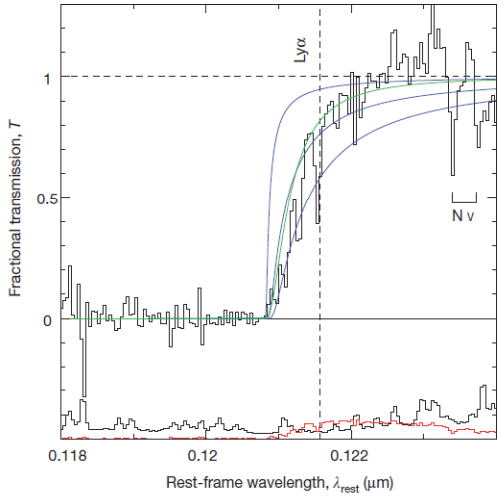

Figure 4 | Rest-frame transmission profile of ULAS J1120+0641 in the region of the Lyα emission line, compared to several damping profiles. The transmission profile of ULAS J1120+0641, obtained by dividing the spectrum by the SDSS composite shown in Fig. 1, is shown in black. The random error spectrum is plotted below the data, also in black. The positive residuals near 0.1230 μm in the transmission profile suggest that the Lyα emission line of ULAS J1120+0641 is actually stronger than average, in which case the absorption would be greater than illustrated. The dispersion in the Lyα equivalent width at a fixed C IV equivalent width of 13% quantifies the uncertaint
profile is s
intergalact
$f_{H1} = 0.5$ a
the quasar
absorber c
the quasar
transparer
might be sufficient to discriminate between these two models[25,27]. The wavelength of the Lyα transition is shown as a dashed line; also marked is the N v doublet of the associated absorber referred to in the text.

Blue: sharp ionizing front at 2.2Mpc with fHI=0.1, 0.5, 1.0
Green: DLA 2.6Mpc away.

When ?

Decrease of the fraction of strong Ly-alpha emitting galaxies (LAE) among z~7 galaxies selected with “dropout” method (Lyman Break Galaxies) suggests that “the neutral fraction of the IGM significantly increases from z~6 to 7 (Ono et al. 2012, also Schenker et al. 2012).

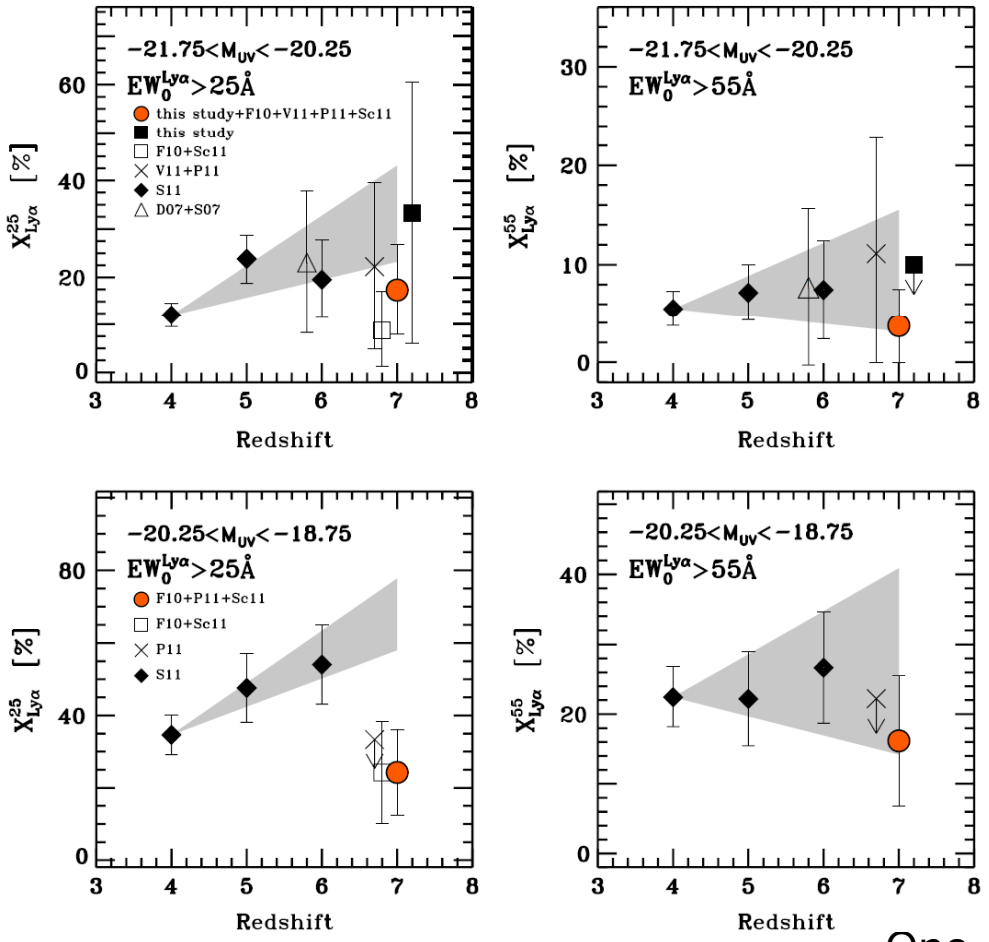

UV-luminous

Less UV-luminous

Ono et al. 2012

When ?

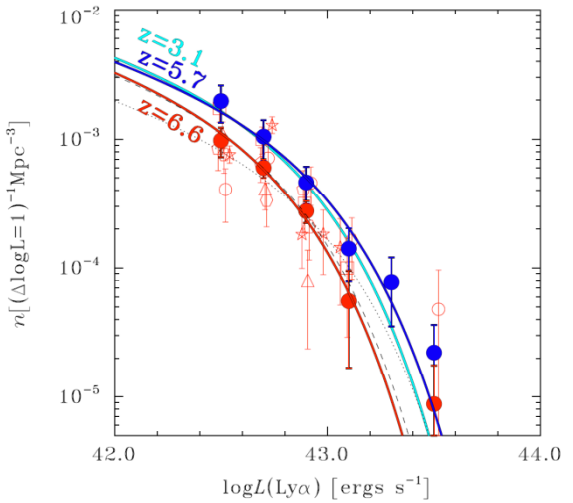

Figure 7. Evolution of Lyα LFs up to $z = 6.6$. Red filled circles are the best estimates of $z = 6.6$ LAEs from the entire SXDS sample and red solid line is the best-fit Schechter function of $z = 6.6$ LAEs. Blue filled circles and the solid line are data points and the best-fit Schechter function, respectively, of $z = 5.7$ LAEs given by Ouchi et al. (2008). Note that the error bars of $z = 6.6$ and 5.7 data points (red and blue filled circles) represent uncertainties from statistics and cosmic variance. The cyan solid line is the best-fit Schechter function of $z = 3.1$ LAEs (Ouchi et al. 2008). The LF decreases from $z = 5.7$ to 6.6 significantly, while no significant evolution can be found between $z = 3.1$ and 5.7. For comparison, we plot LF estimates from each of the five $\sim$0.2 deg^2 subfields with the same open symbols as found in Figure 6. These open symbols illustrate that with the data of a single $\sim$0.2 deg^2 field alone (e.g., open circles down to $\log L_{\mathrm{Ly}\alpha} \simeq 42.6$), which is a typical survey size of previous studies, it is difficult to distinguish whether or not $z = 6.6$ LFs show evolution (decrease) with respect to $z = 5.7$. Dashed and dotted lines represent the best-fit Schechter functions to our $z = 6.6$ LF with a ϕ^* and L^* fixed to that of $z = 5.7$, respectively.

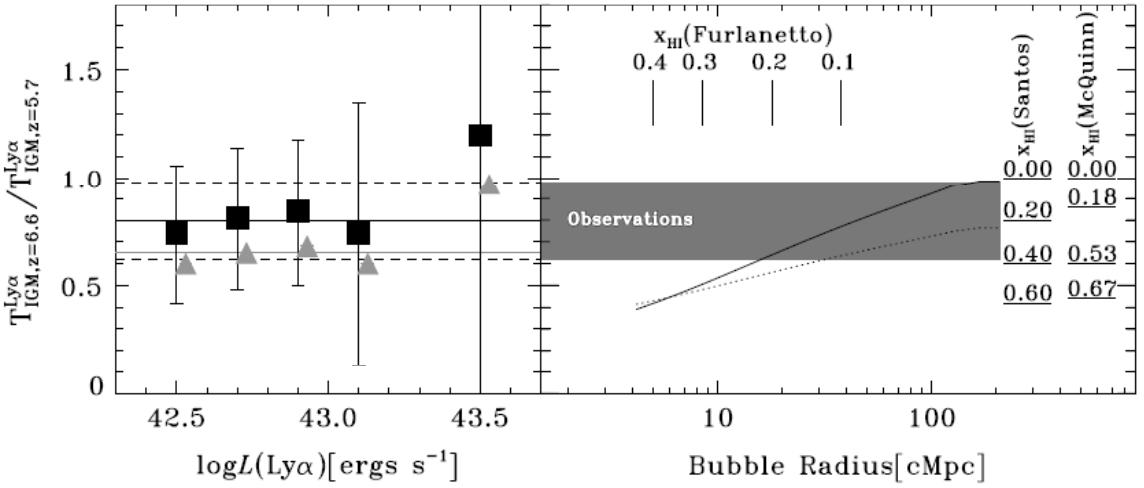

Figure 20. Lyα transmission through IGM at $z = 6.6$ that is normalized by the one at $z = 5.7$. Left panel shows our observational estimates of $T^{\mathrm{Ly}\alpha}_{\mathrm{IGM},z=6.6}/T^{\mathrm{Ly}\alpha}_{\mathrm{IGM},z=5.7}$. Black squares plot $T^{\mathrm{Ly}\alpha}_{\mathrm{IGM},z=6.6}/T^{\mathrm{Ly}\alpha}_{\mathrm{IGM},z=5.7}$ in the case of no evolution of Lyα escape fraction ($f^{\mathrm{Ly}\alpha}_{\mathrm{esc}}$). Black solid and dashed lines are the best estimate and $\pm 1\sigma$ errors of $T^{\mathrm{Ly}\alpha}_{\mathrm{IGM},z=6.6}/T^{\mathrm{Ly}\alpha}_{\mathrm{IGM},z=5.7}$, respectively, for the no $f^{\mathrm{Ly}\alpha}_{\mathrm{esc}}$ evolution case. Similarly, gray triangles and line represent the lower limit in the case of the $f^{\mathrm{Ly}\alpha}_{\mathrm{esc}}$ evolution. Right panel compares these estimates with model predictions. Gray region shows our observational constraints ($\pm 1\sigma$) on $T^{\mathrm{Ly}\alpha}_{\mathrm{IGM},z=6.6}/T^{\mathrm{Ly}\alpha}_{\mathrm{IGM},z=5.7}$. Solid and dotted lines represent the model predictions of Dijkstra et al. (2007b) as a function of ionized bubble radius in comoving Mpc for the cases with and without ionizing background boosts of undetected surrounding sources, respectively. Ticks at the top present the relation between the typical bubble radius and the neutral-hydrogen fraction of IGM for $x_{\mathrm{H\,I}} \simeq 0.4$, 0.3, 0.2, and 0.1, which are predicted by the analytic model of Furlanetto et al. (2006). Two sets of ticks in the right-hand side of the panel denote the predicted relations between $x_{\mathrm{H\,I}}$ and $T^{\mathrm{Ly}\alpha}_{\mathrm{IGM},z=6.6}/T^{\mathrm{Ly}\alpha}_{\mathrm{IGM},z=5.7}$ in the models of Santos et al. (2004) and McQuinn et al. (2007).

Ouchi et al. 2010

Who ?

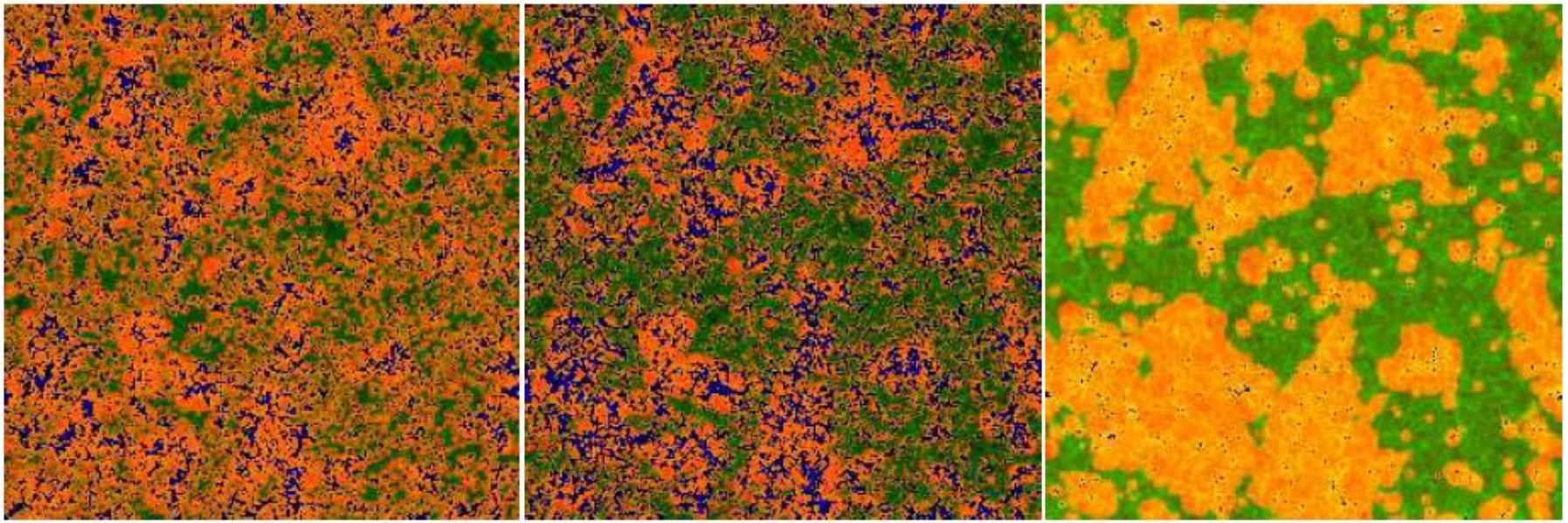

Figure 11. Spatial slices of the ionized and neutral gas density from our radiative transfer simulations with boxsize 163 Mpc: (a)(left) L1 (b)(middle) L2, and (c)(right) L3, all at box-averaged ionized fraction by mass of $x_m \sim 0.50$. Shown are the density field (green) overlayed with the ionized fraction (red/orange/yellow) and the cells containing active sources (dark/blue).

Iliev et al. 2012

Structure of re-ionization can be different whether the ionizing photons are from galaxies associated with numerous low-mass halos (left) or rare high-mass halos (right).

(163Mpc box ~ 1deg scale)

Who ?

- Models of UV luminosity function of high-redshift galaxies suggests that contribution from numerous low-mass halo (= low-luminoisty galaxies) is important.

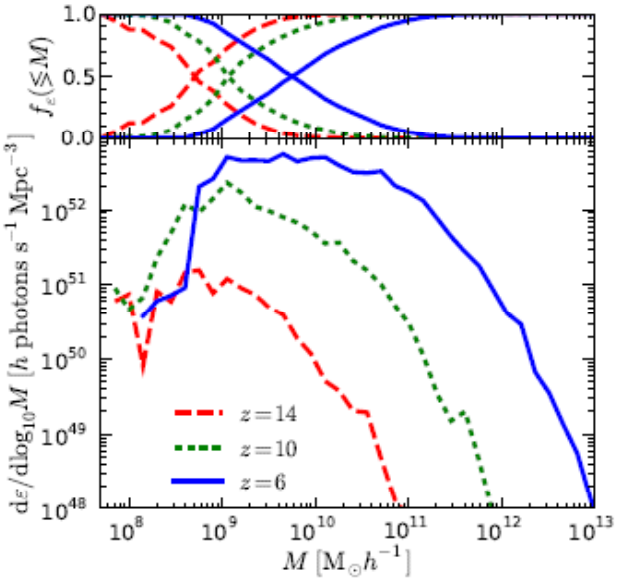

Figure 3. *Main panel*: Lyman-continuum emissivity as a function of halo mass, $\mathrm{d}\epsilon(M,z)/\mathrm{d}\log_{10}(M)$, for various redshifts indicated in the panel. The emissivity is low for very low-mass halos that are unable to cool gas, reaches a peak which increases with decreasing z, and a tail towards larger masses set by the exponential drop in the number of massive halos. At $z \sim 10$ most ionizing photons are produced by halos in a relative small mass range, ~ 1 dex. *Top inset*: cumulative fraction f_c of ionizing photons produced in halos more massive or less massive than a given value (rising and falling curves, respectively). The mass of halos below which 50 per cent of ionizing photons is produced rises by approximately an order of magnitude from $\sim 8 \times 10^8\, h^{-1}\mathrm{M}_\odot$ at $z = 14$ to $\sim 8 \times 10^9\, h^{-1}\mathrm{M}_\odot$ at $z = 6$.

Raicevis et al. 2010

Who ?

Observed UV luminosity functions of dropout galaxies show steep faint-end slope and the numerous faint galaxies can ionize the universe.

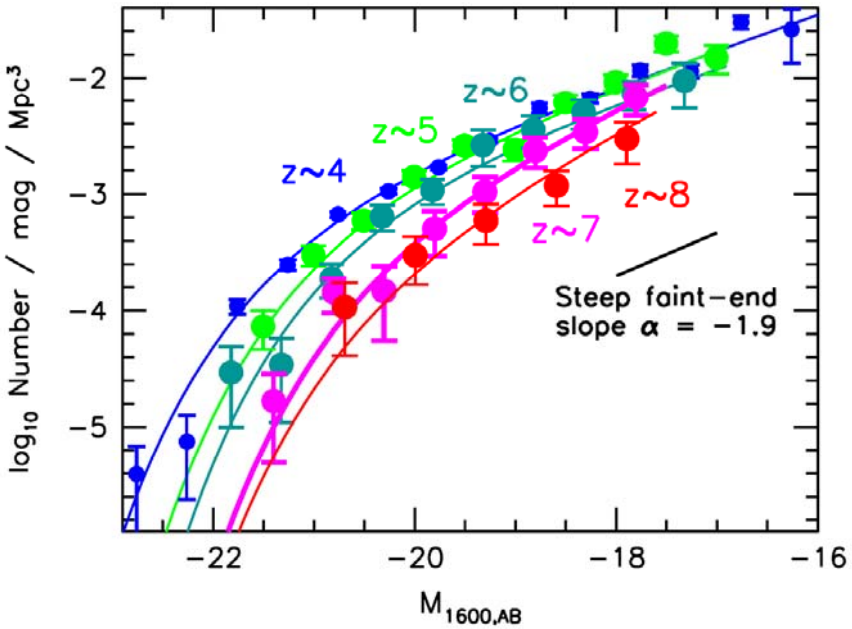

Figure 1. *UV* luminosity functions at $z \sim 4$, $z \sim 5$, $z \sim 6$, $z \sim 7$, and $z \sim 8$ (Section 3). The solid circles represent the stepwise maximum-likelihood determinations while the solid lines are the Schechter function determinations (they are *not* fits to the points, though the overall agreement is excellent). The $z \sim 4$ constraints are from Bouwens et al. (2007). The new $z \sim 5$ (green) and $z \sim 6$ (cyan) results are from the present work, while the $z \sim 7$ (magenta) and $z \sim 8$ (red) points are from Bouwens et al. (2011b).

Bouwens et al. 2012

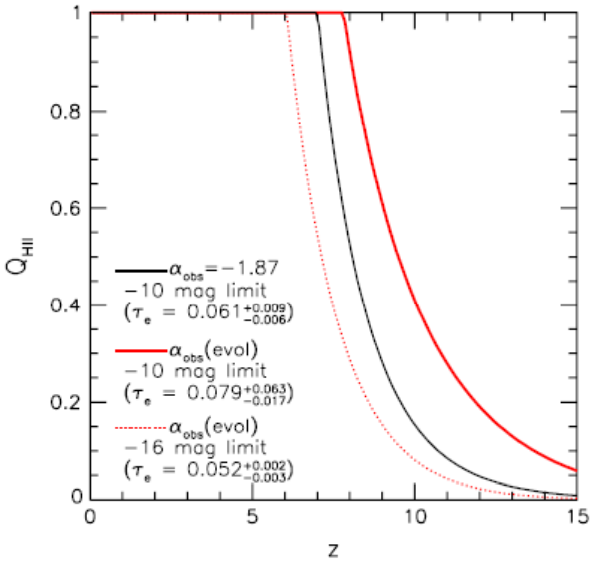

Figure 3. Filling factor of ionized hydrogen $Q_{\rm H\,II}$ vs. redshift using our LF-fitting formula for *UV* LF at $z \geqslant 4$ (Table 1). The respective ionization histories (represented by the lines) were calculated from Equation (2) assuming a Lyman-continuum escape fraction $f_{\rm esc}$ of 20%, a clumping factor of three, an IGM temperature of 2×10^4 K, a 1/50 $Z_\odot$ Salpeter initial mass function, and assuming the LF extends down to −10 mag (with the same faint-end slope α). See the text for references and see also Figure 8 from Bolton & Haehnelt (2007) and Figure 4 from Oesch et al. (2009). The solid black line shows the filling factor derived from best-fit LF (Figure 2 and Table 1; Section 4) with the mean faint-end slope $\alpha = -1.87 \pm 0.13$ found at $z \sim 6$–8 and for the best-fit evolution in α. The Thomson optical depths τ for these ionization histories are $0.061^{+0.009}_{-0.006}$ and $0.079^{+0.063}_{-0.017}$, respectively. The red dotted line is for our best-fit faint-end slope α evolutionary scenario, but assumes the LF extends to just −16 mag (the limit of our data) showing that while observed galaxies can reionize the universe by $z \sim 6$, they produce τ, i.e., $0.052^{+0.002}_{-0.003}$, which are too low. Changes in the adopted cosmology also affect the derived τ. Allowing for evolution of the faint-end slope and a faint-end limit of −10 mag to the LF, we find an optical depth easily consistent with the $\tau = 0.088 \pm 0.015$ found by *WMAP* (Komatsu et al. 2011). This suggests that star-forming galaxies in the first 700–800 Myr could reionize the universe.

How ?

- Observations of ionizing continuum photons from z~3 galaxies (Steidel et al. 2001, Shapley et al. 2006, Iwata et al. 2009) suggest higher escape fraction (fesc~0.04-0.20) for galaxies at high-redshifts than for those for galaxies at intermediate redshifts.

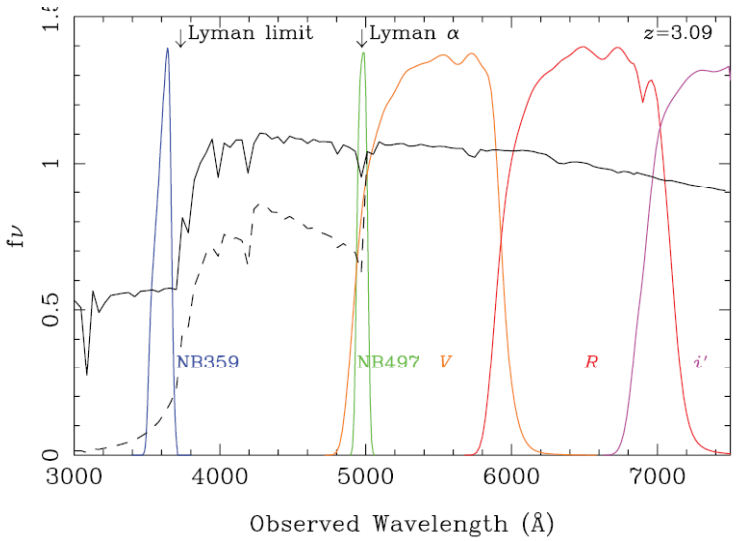

Figure 1. Filter transmission curves for the filters used in this study and spectra of a model star-forming galaxy at $z = 3.09$ generated with the Starburst99 code. The solid line represents a model without IGM attenuation, and the dashed line is for a model with average IGM attenuation for objects at $z = 3$. See Section 4.3 for details of the model.

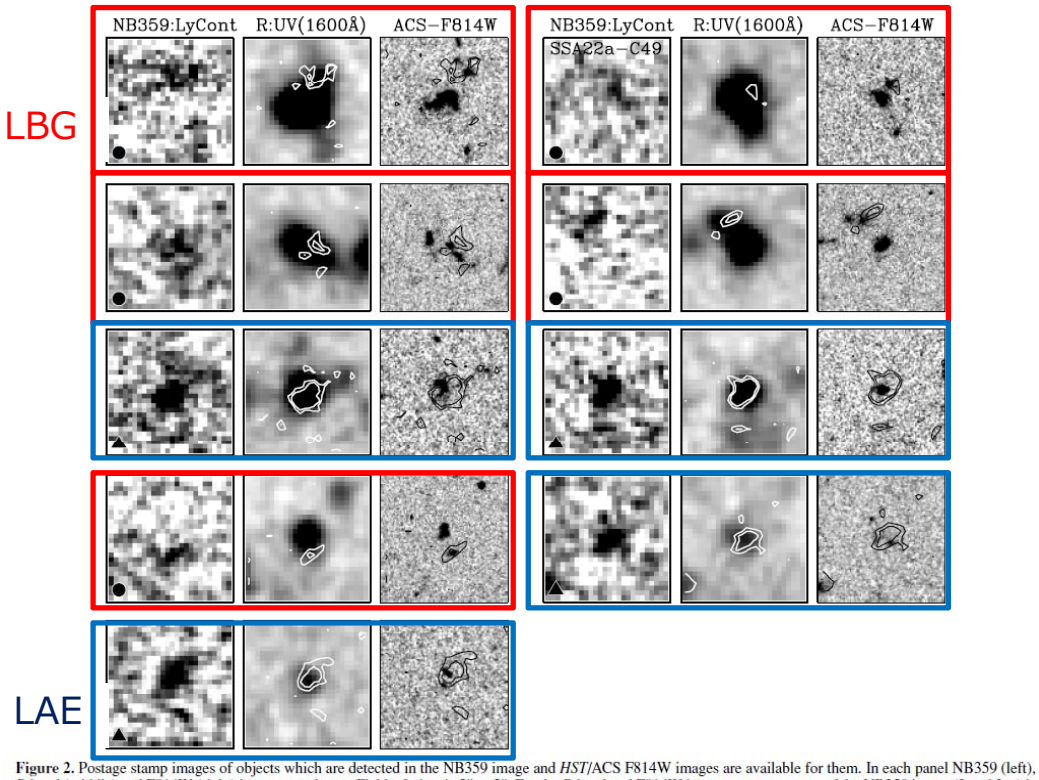

Figure 2. Postage stamp images of objects which are detected in the NB359 image and *HST*/ACS F814W images are available for them. In each panel NB359 (left), *R*-band (middle) and F814W (right) images are shown. Field-of-view is 5″ × 5″. For the *R*-band and F814W images a contour map of the NB359 image (2 and 3 σ) is overplotted. Symbols at the lower left of the NB359 images show the object type: filled circles: LBG; filled triangle: "blue" LAEs. See Section 4.3 for the definition of types. The images of SSA22a-C49, which is one of the two objects reported to be detected in S06 and is detected in our NB359 image with 2.95σ level, is labeled.

Iwata et al. 2009

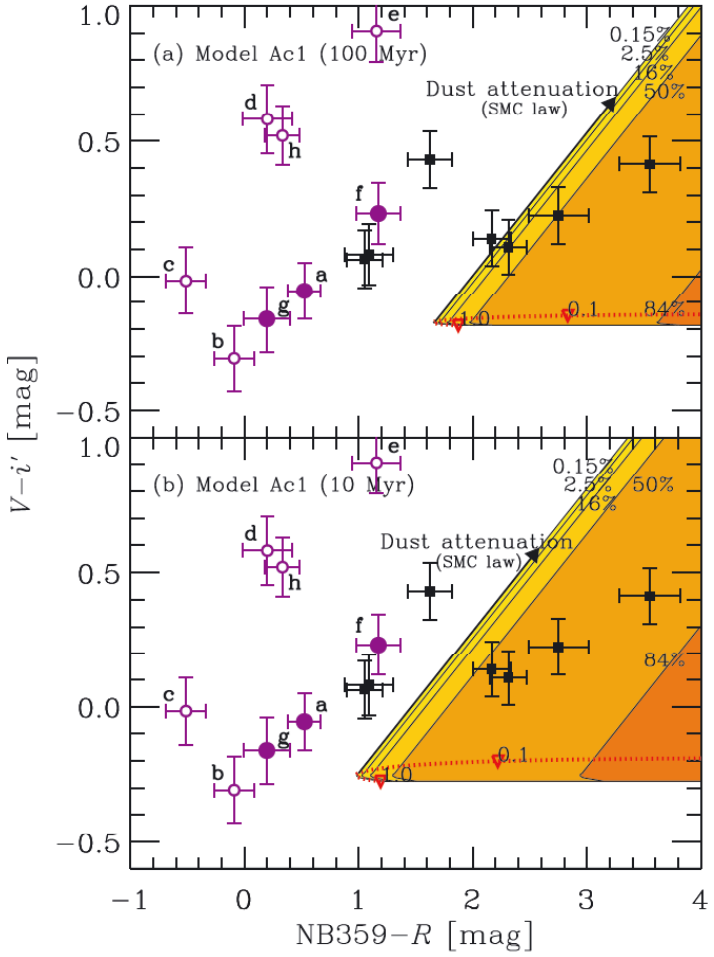

Figure 10. Same as Fig. 6 but a comparison with the escaping nebular LyC scenario of a continuous star-forming galaxy with $Z = 1/50\,Z_{\odot}$ (model Ac1). (a) age from the or Myr. The dotted curves indica cape fraction of stellar LyC w ıbols indicate the positions w The shaded regions indicate t IGM and dust attenuations. From thin to thick, the cumulative probability to have the amount of the IGM attenuation increases. The SMC extinction law is adopted for the dust attenuation as shown by the solid arrow. The nebular gas temperature is assumed to be 1×10^4 K.

Black : LBG
Purple : LAE
Inoue et al. 2011

How ?

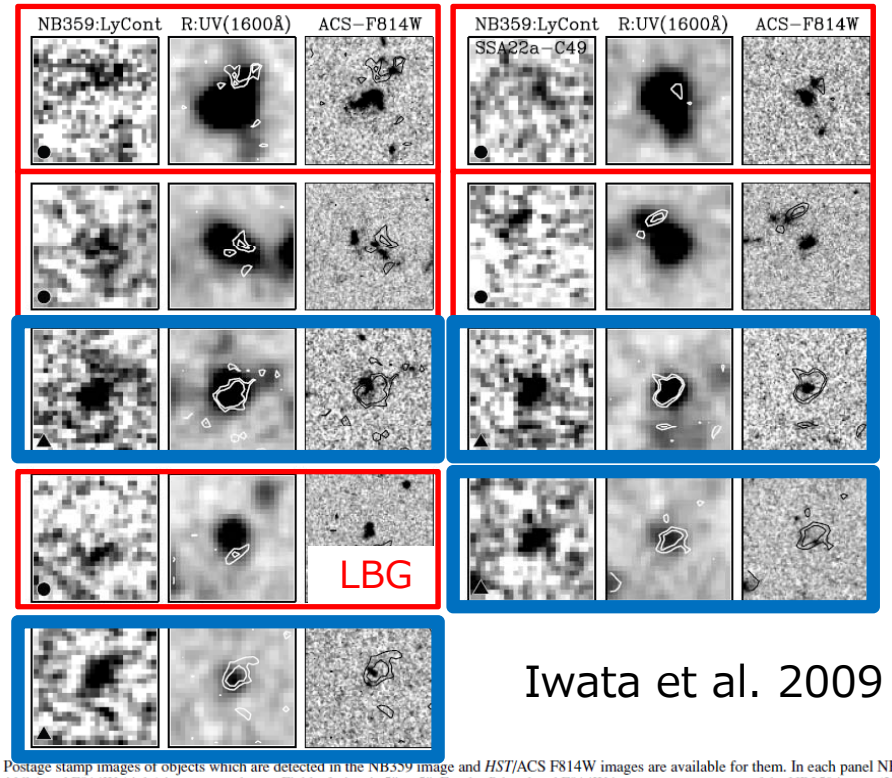

Iwata et al. 2009

Figure 2. Postage stamp images of objects which are detected in the NB359 image and *HST*/ACS F814W images are available for them. In each panel NB359 (left), *R*-band (middle) and F814W (right) images are shown. Field-of-view is $5'' \times 5''$. For the *R*-band and F814W images a contour map of the NB359 image (2 and 3 σ) is overplotted. Symbols at the lower left of the NB359 images show the object type: filled circles: LBG; filled triangle: "blue" LAEs. See Section 4.3 for the definition of types. The images of SSA22a-C49, which is one of the two objects reported to be detected in S06 and is detected in our NB359 image with 2.95σ level, is labeled.

- Some Lyman Alpha Emitters show even stronger Lyman continuum emission (NB359) and have blue NB359-R color.
- Such blue color cannot be explained with usual young stellar population (1/50 Zsoloar, 10-100Myr). Very young (1Myr), very metal poor, and massive (~100Msolar) stellar population may be necessary.

Re-ionization of the Universe

Understandings of the re-ionization of the universe;

- When ?
- Who ?
  - Galaxies or AGNs ? = stars or black holes ?
  - Massive galaxies or less-massive galaxies ?
- How ?
  - Escape fraction of ionizing photons from galaxies
  - Relation with clumping factor of neutral gas distribution

<u>Understanding of the physical conditions and processes of formations of stars and black holes in the early Universe.</u>

Frontier of Subaru (-related) studies

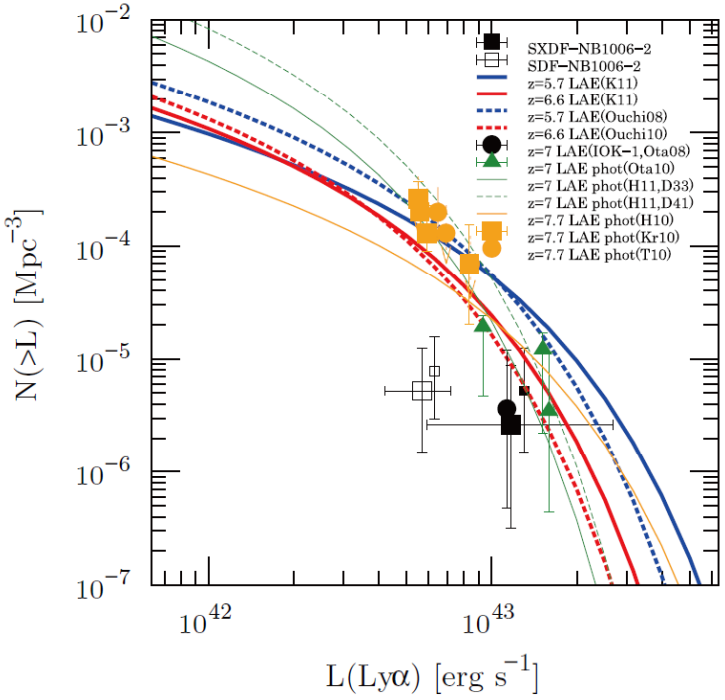

z=7.3 LAE
Subaru Scam(red-sensitive CCD)
NB1006, 22h exp.
FWHM 0.98”
24.83mag (5sigma)
(Shibuya et al. 2012)

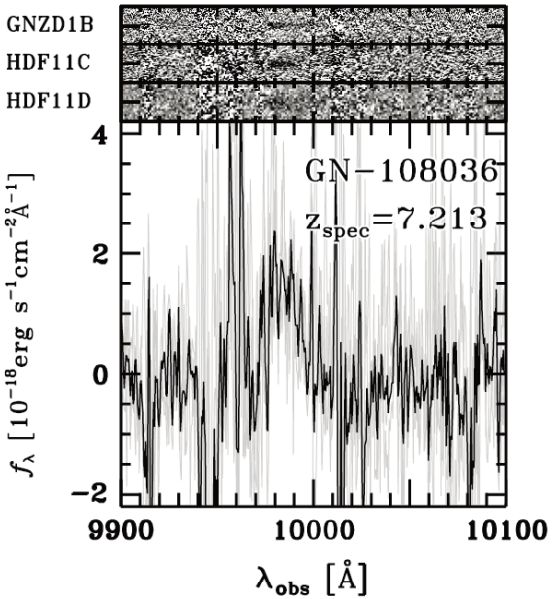

Figure 2. Spectrum of the $z = 7.213$ z-dropout galaxy, GN-108036. The top panels show its two-dimensional spectra obtained with the GNZD1B, HDF11C, and HDF11D masks. The size along the spatial axis is 5″.0 for each two-dimensional spectrum. The HDF11D spectrum is binned in 2×2 pixels. A line is visually identified at ≃9980 Å in the spectra of GNZD1B and HDF11C, whose exposure times are 5 hr and ≃4 hr, respectively, while the line is marginally seen in the spectrum of HDF11D, whose exposure time is 2 hr. In the bottom panel, we show the one-dimensional spectra. The gray solid lines are spectra obtained with individual masks. The composite spectrum is shown as the black solid line. All the one-dimensional spectra illustrate a line detection at around 9980 Å, and the S/N of the line in the composite spectrum is ≃6.

z=7.2 LBG
Keck DEIMOS, 11h exp.
fLya=2.5e-17 erg/s/cm2
Llya=1.5e+43 erg/s
(Ono et al. 2012)

Tomorrow and the day after tomorrow

- Probing at z~7 with better statistics with large and deep imaging surveys with Hyper Suprime-Cam.

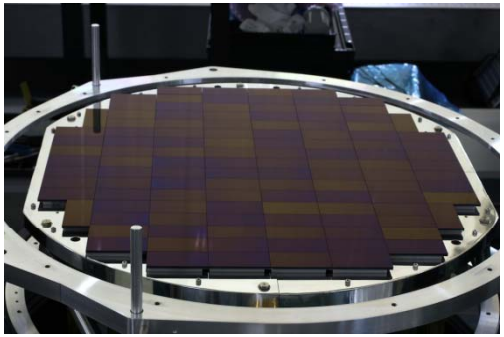

From Subaru webpage
Commissioning run stars this fall

- Probing at higher redshifts by wide-field NIR imager with Ground-layer AO !
  - Subaru's studies on GLAO systems and feasibility of probing galaxies at higher redshifts (z>7).
  - Results are applicable to GLAO system on Gemini.

GLAO simulation summary

Simulations suggest…

- Relatively good image size can be obtained even in short wavelength range (~8000A). No significant halo component expected ?
- High throughput can be achieved even with small apertures; typically we can half the slit width (MOIRCS w/o AO 0.8″ to 0.4″). 4 times smaller background expected.

<u>FWHM</u>
Blue: 10′
Green: 15′
Red: 20′

<u>Ensquared E.</u>
blue: 0.24″
green: 0.36″
red: 0.48″

By Shin Oya
(Subaru, NAOJ)

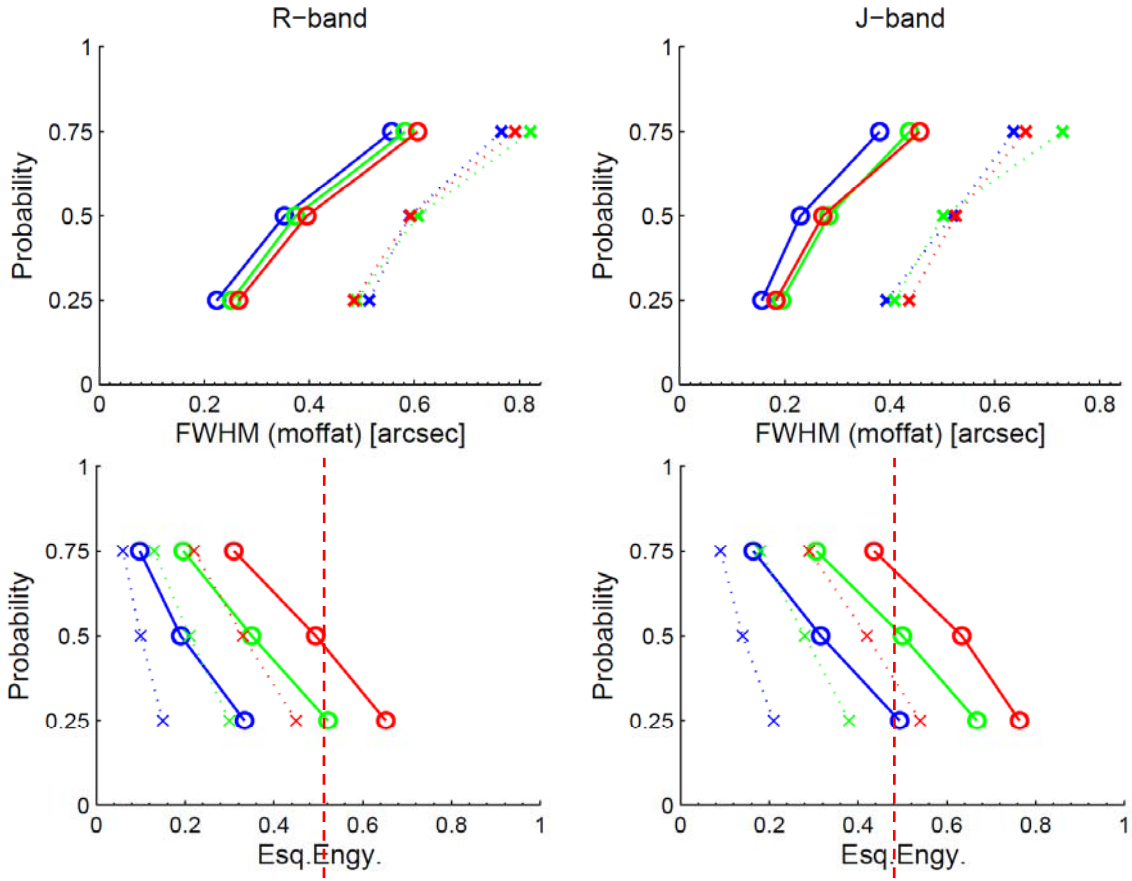

Survey comparison

Calculations conducted by Ikuru Iwata (Subaru, NAOJ) based on Shin Oya (Subaru, NAOJ) GLAO simulated PSF

	Mirror [m]	Pix scale ["/pix]	FoV [arcmin2]
Subaru / MOIRCS	8.2m	0.117	28
Subaru / GLAO+WFI	8.2m	0.117	177
JWST / NIRCam	6.5m	0.0317	9.68
WISH	1.5m	0.155	840

For Subaru GLAO+WFI, three narrow band filters are assumed,

NB106 10600A with top-hat filter with d=150A targetting LAEs @ z=7.7

Co-moving volume: 5.0e+3 Mpc^3 / fov

NB134 13400A with top-hat filter with d=190A targetting LAEs @ z=10.0

Co-moving volume: 4.0e+3 Mpc^3 / fov

NB155 15500A with top-hat filter with d=220A targetting LAEs @ z=11.8

Co-moving volume: 3.4e+3 Mpc^3 / fov

JWST has narrow-band filter above 16000A

WISH is a wide-field IR imaging survey satellite proposed by T. Yamada et al. (Tohoku Univ.)

Broad-band limiting magnitude (5sigma, AB) with 10^4s exp.

For broad-band imaging, observation from space can achieve much deeper flux limit thanks to low-background level or no OH line. (Ground-based observations have advantage in the size of FoV.)

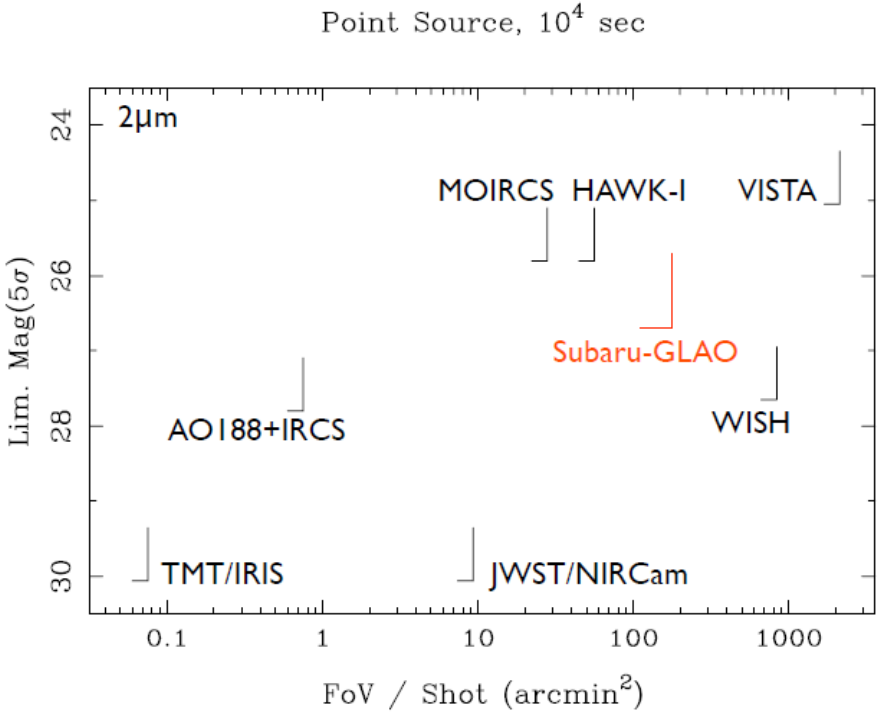

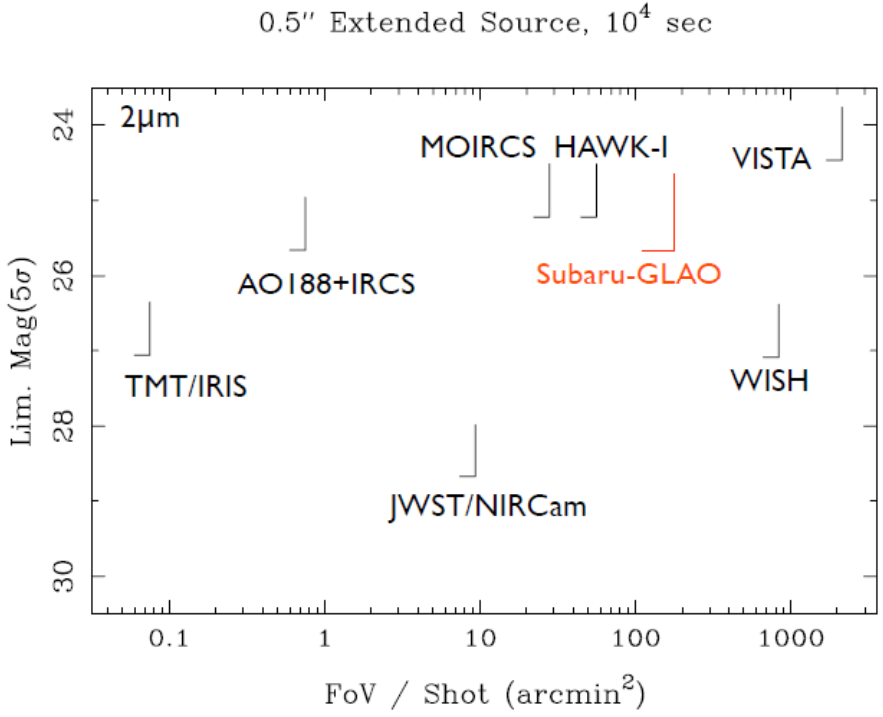

By I.Iwata

NBF limiting magnitude (10sigma, AB) with 10h exp.

If narrow-band observation in between strong OH lines is assumed, ground-based observation can reach similar depth to the observation from space.
So continuum selections (like dropout) is better from space, but line selections (like Ly-alpha emitter) can be done efficiently from ground.

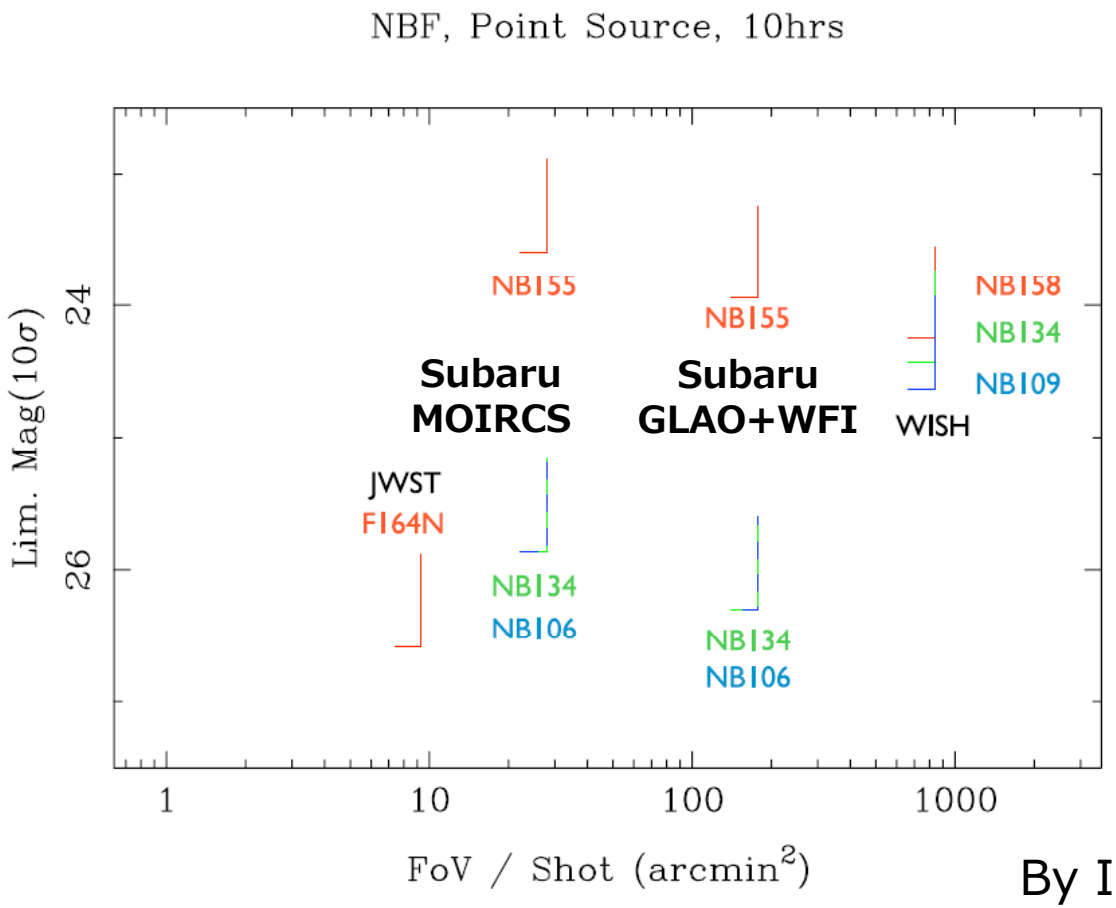

By I.Iwata

Detection limit with 10h exp.

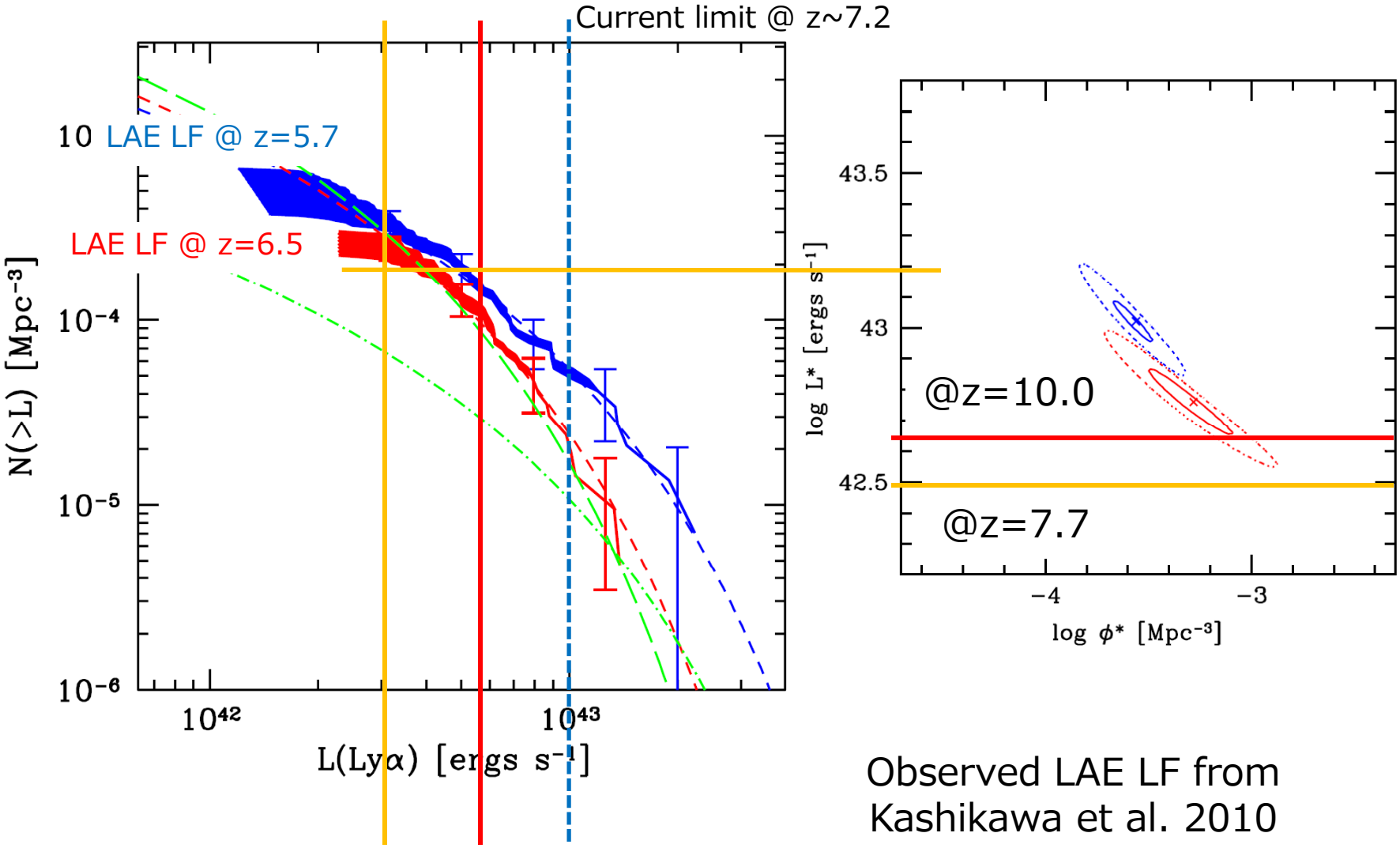

@z=7.7 @z=10.0

Subaru GLAO+WFI 10h limit

Observed LAE LF from
Kashikawa et al. 2010

Detection limit with 10h exp.

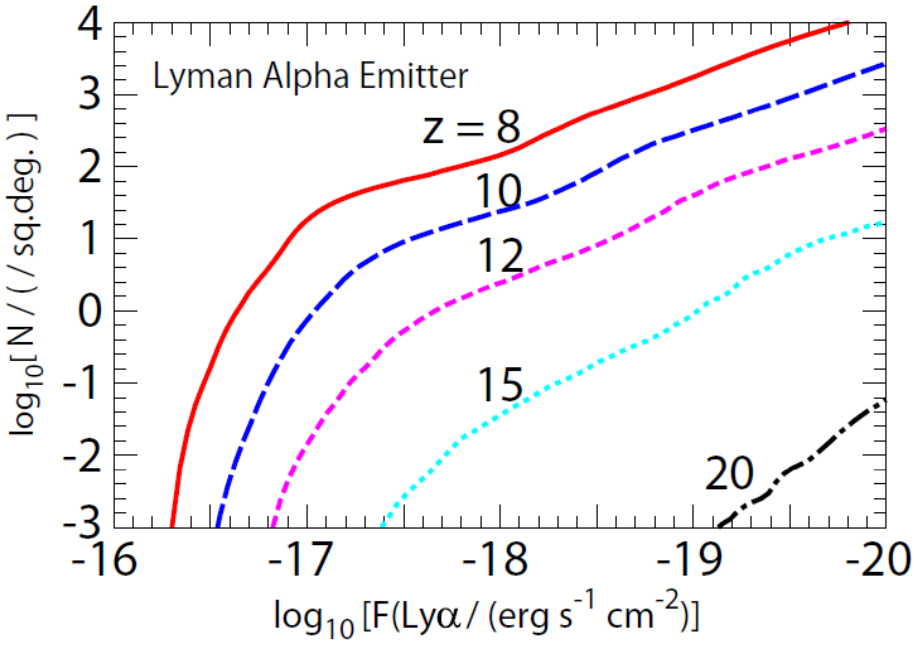

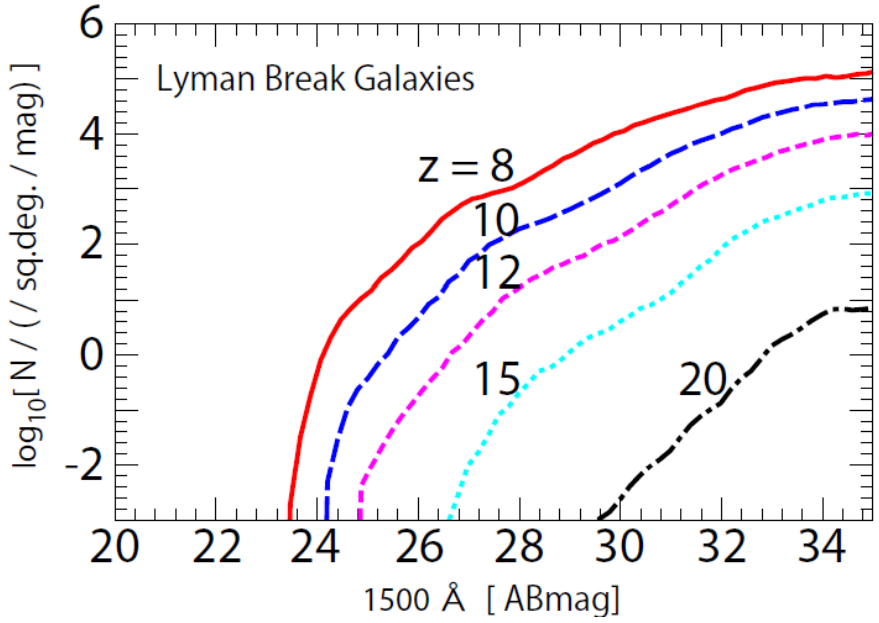

Semi-analytic models of LAE
and LBG number counts
(Kobayashi et al. 2010)

Expected number per FoV with 10h exp.

No Evolution from z=6.5 i.e., ~Maximum Number

	Number / FoV			
	Seeing	GLAO	WISH	JWST
z~8	0.5	8.3	0.2	--
z~10	0.2	3.3	0.01	--
z~12	3E-08	8E-06	7E-04	0.3

Subaru GLAO+WFI

Based of SAM by Kobayashi et al.

	Number / FoV		
	Seeing	GLAO	JWST
z~8	0.4	3.9	--
z~10	0.03	0.5	--
z~12	~0	~0	0.003

Subaru GLAO+WFI

By I.Iwata

- The number density of LAEs brighter than L* can be constrained up to z~10.
  - Good constraints on the ionized fraction in the redshift range.
  - Further studies (Ly-alpha line profile, stellar population) can be done with >30m telescopes.

Wide field of view is crucial…

Galaxies@z~6 show strong clustering in 100Mpc (~0.7deg) scale.

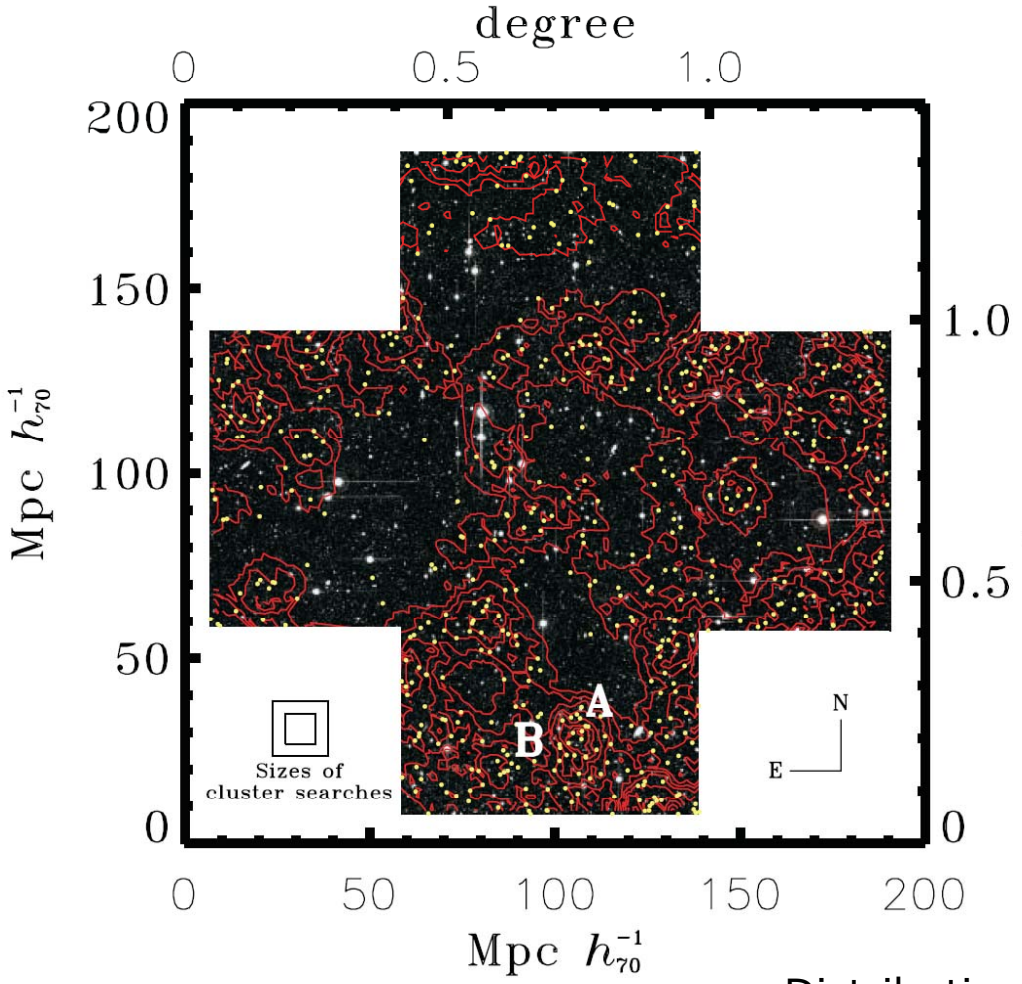

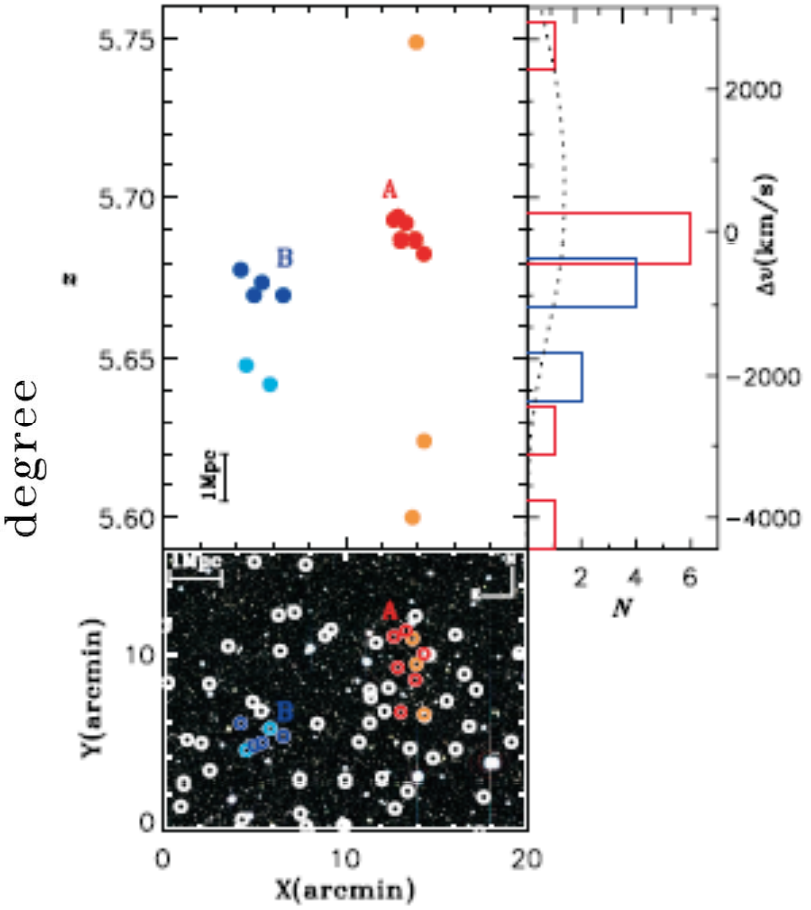

Distribution of z~5.7 LAEs and discovery of a proto-cluster (Ouchi et al. 2005)

Wide field of view is crucial…

Galaxies@z~6 show strong clustering in 100Mpc (~0.7deg) scale.

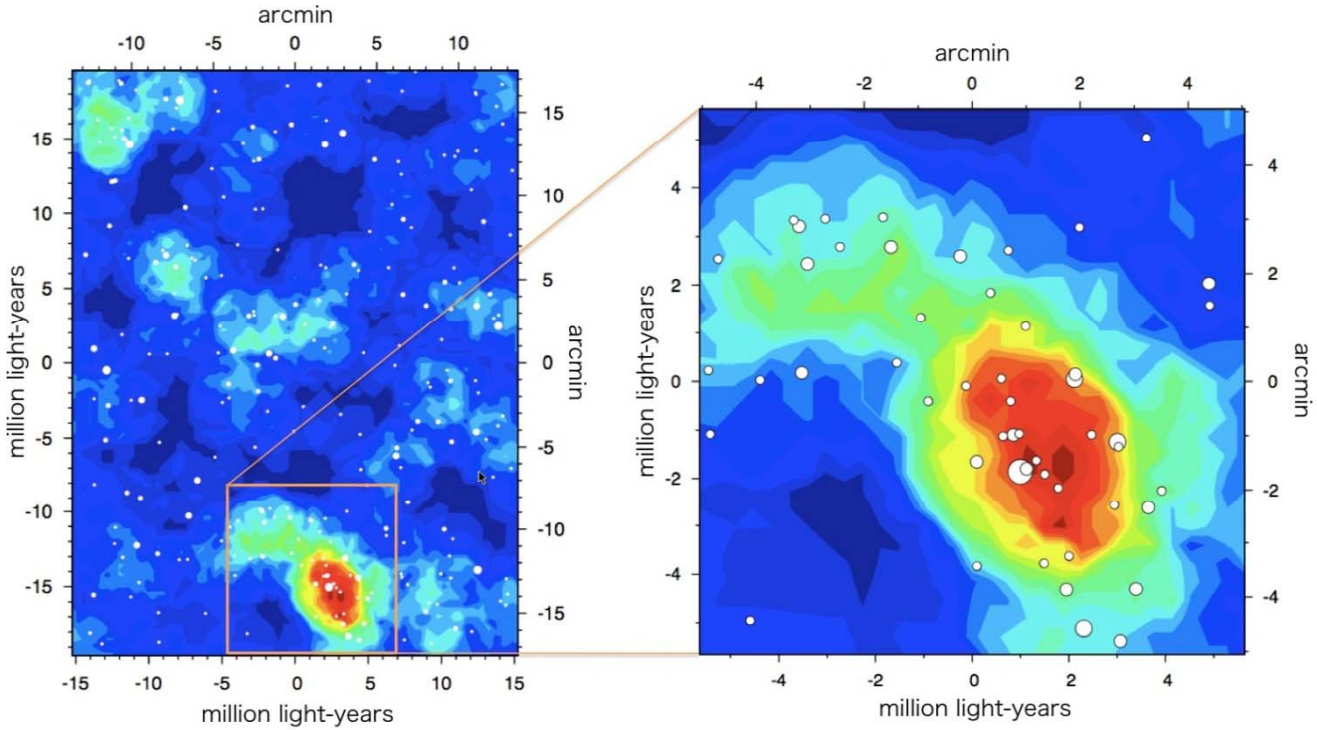

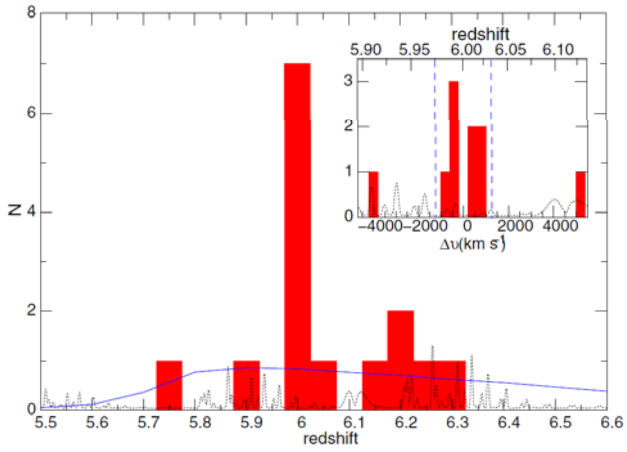

Distribution of z~6 LBGs and discovery of a proto-cluster at z=6 (Toshikawa et al. 2012)

High Strehl Ratio is not crucial…

- Average sizes of galaxies at high-redshifts are ~0.2″, GLAO-like correction is sufficient to improve the detection limit.

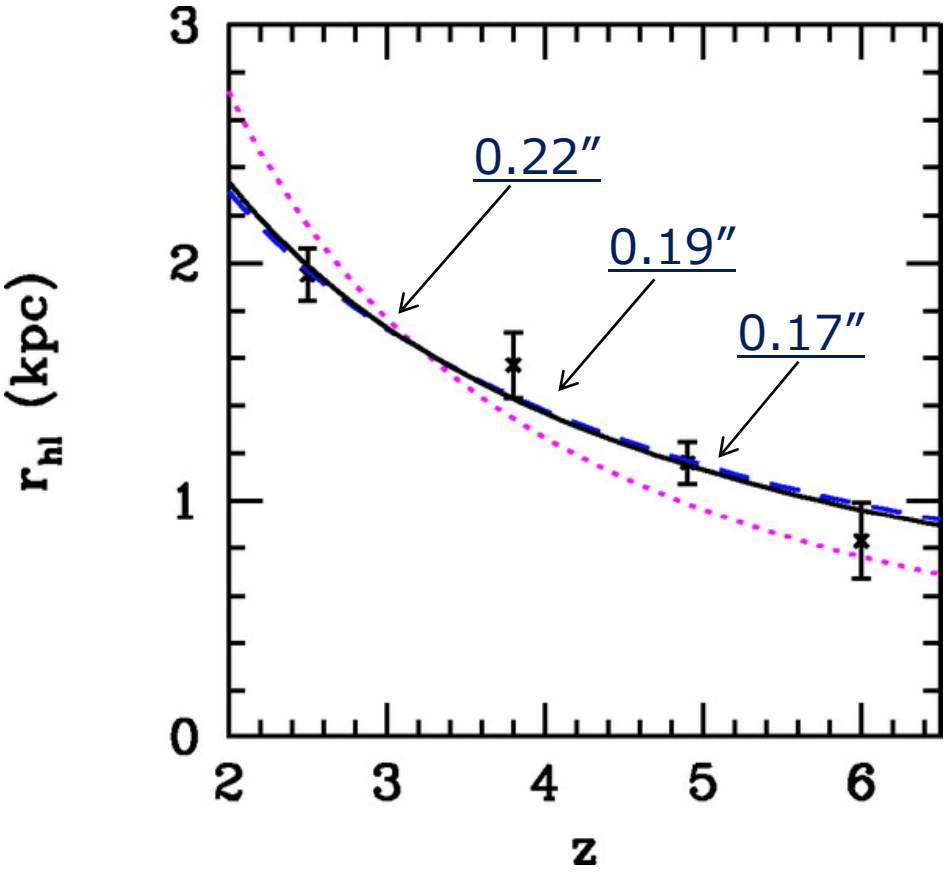

Bouwens et al. 2004, ApJ, 611, L1

AO: feedback

- GLAO system with wide field camera on 8m-class telescope can conduct narrow-band survey for Lyman Alpha Emitters at even higher redshifts.
  - ✓ Field of view should be as wide as possible.
  - ✓ AO-correction with FWHM~0.2” is sufficient.
  - ✓ AO-correction in relatively short wavelength (z, Y, J-bands) range is important.
- High-throughput (in z, Y, J-band = in the middle of CCD and IR-detectors) and large sky coverage AO-supported (single object) spectrograph is necessary for the spectroscopic follow-ups. AO-correction like LGS+P1 mode on Gemini sounds promising.

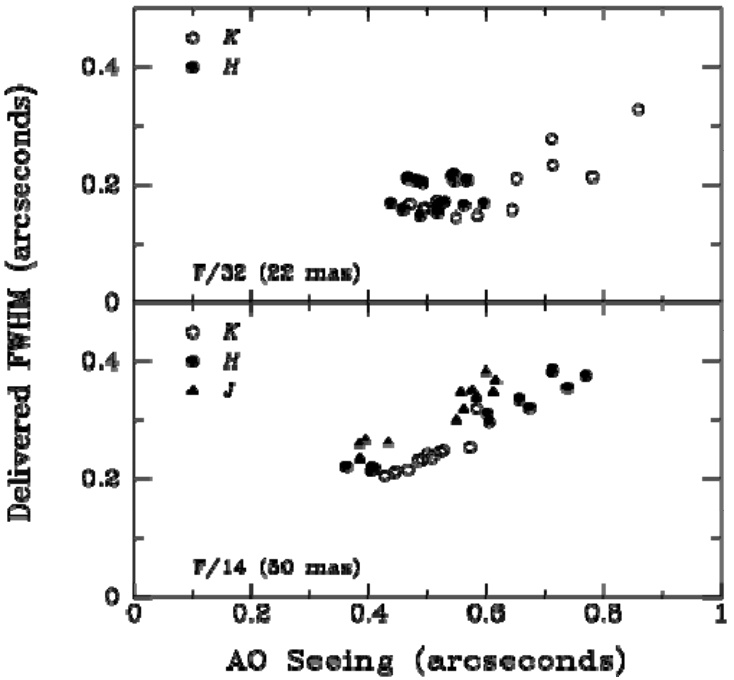

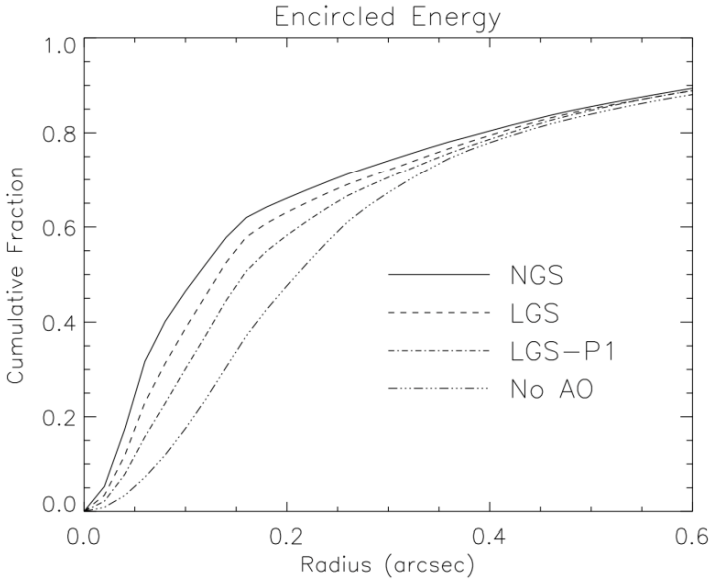

From Gemini web-site

What's your favorite AO flavor ?

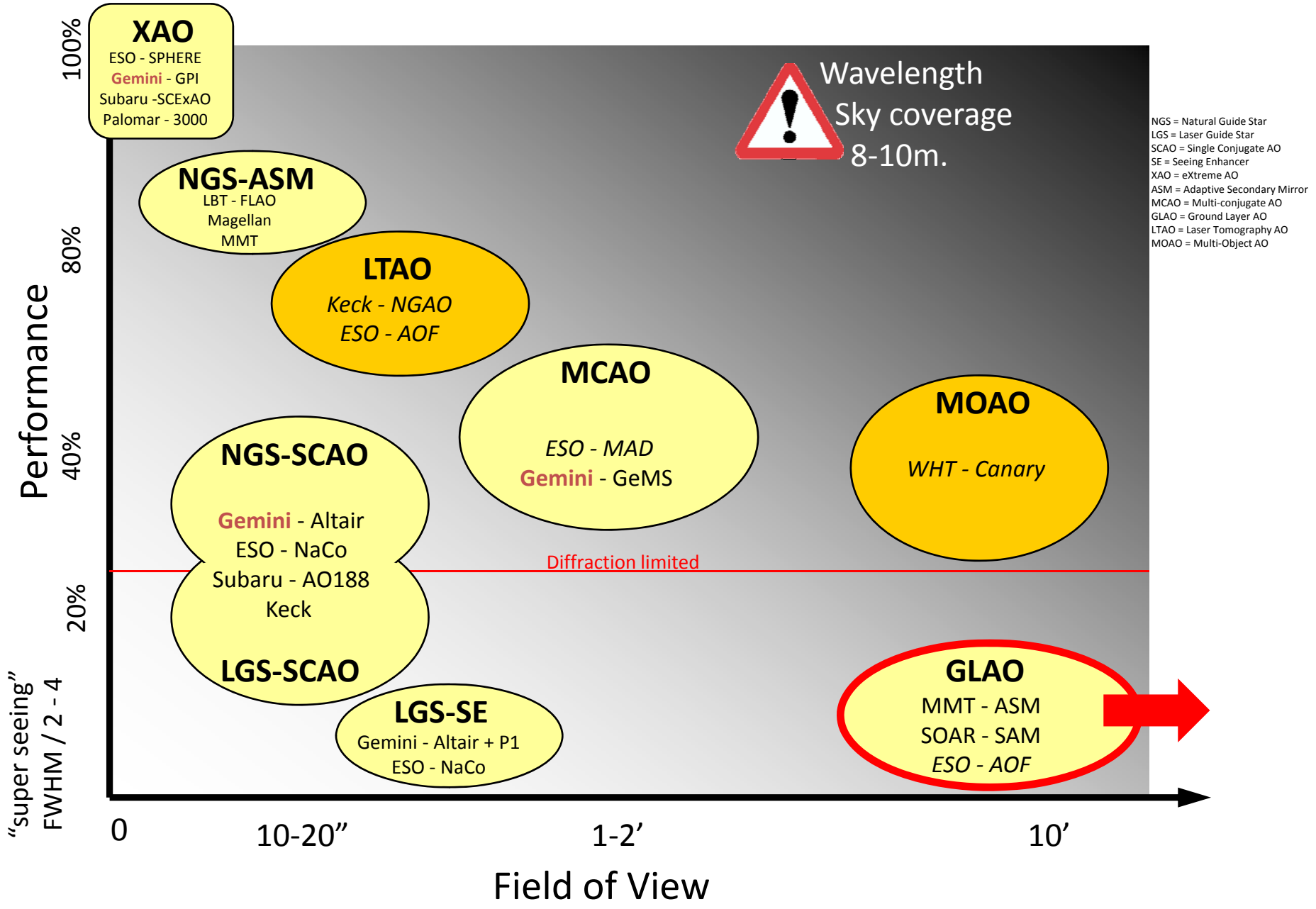

My summary from Subaru NGAO WS (2010/09)

Deep observation of an individual object: Good synergy with HSC database

Spectroscopic follow-up of high-redshift galaxies: Lya emitter @ z=7

High-SN, medium-resolution spec. : Gun-Peterson trough of z=6-7 QSOs

High-SR (0.6-0.7 @ K-band)
= Shorter wavelength range (~9000A)
High sky coverage (>50% : GS:R=18mag,60”,1GS)

Direction 1
~ Keck-NGAO
~ Gemini-GEMS

Deep observation of multiple objects: Extending FMOS,MOIRCS exp.

Search for galaxines in the early Universe. Good synergy with TMT

Spectroscopic follow-up of red-galaxies: Galaxies, AGNs @ z=1-3

Moderate SR (0.1-0.3 @ K-band ~ 100 elements)
Wide fov (5-10’ scale)

Direction 2

High spacial obs. of an individual object (w/o bright NGS): Real frontier ?

Resolving crowded region in near-by galaxies: AGN, stellar pops in local galaxies

Wavelength as short as possible
Resolution better than HST

Direction 3

Who ?

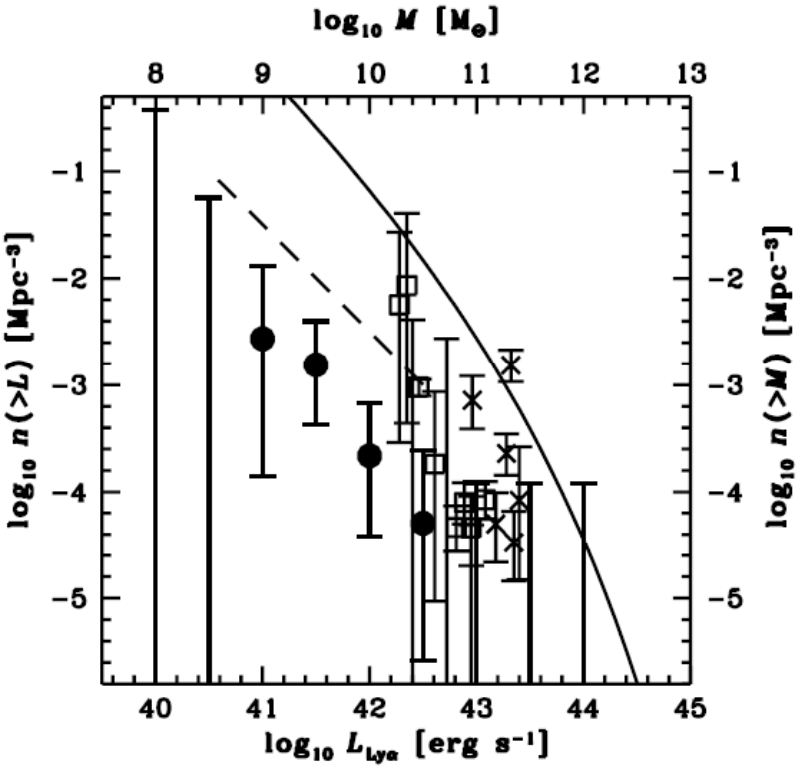

FIG. 13.—Number density of $z \sim 5$ sources brighter than L for Lyα surveys and $z \sim 5$ LBG surveys. The circles are for our cumulative number densities of *confirmed* sources brighter than L for subsurveys within the $4.6 < z < 5.6$ bin (described in Fig. 11). The squares are for the cumulative number densities of sources brighter than L inferred from other $z \sim 5$ Lyα line surveys, and the crosses are for data from $z \sim 5$ LBG surveys. The LBG surveys were converted to equivalent Lyα line luminosities (see § 7.1). The dashed curve shows a prediction from Haiman & Spaans (1999). The solid curve shows the cumulative number density of halos above the total mass given on the top axis; the mass scale (*top axis*) was calibrated to the Lyα luminosity scale using the simple model of § 7.2; the vertical scale is the same (*right axis*). The data are described in Table 3. [*See the electronic edition of the Journal for a color version of this figure.*]

Santos et al. 2004